ASSOCIAZIONE NAZIONALE ITALIANA DI
INGEGNERIA SISMICA
ANIDIS
Italian National Association of Earthquake Engineering

XVIII CONVEGNO ANIDIS
L'ingegneria sismica in Italia
ASCOLI PICENO 2019
15-19 Settembre

N2 with Cloud: A Non-Linear Dynamic Analysis Procedure for the Equivalent SDOF System

Fatemeh Jalayer[a], Hossein Ebrahimian[a], Andrea Miano[a]

[a] Università degli Studi di Napoli Federico II, Dipartimento di Strutture per l'Ingegneria e l'Architettura, Via Claudio 21, 80125 Napoli, Italy

ABSTRACT

The original N2 method for reasonably regular buildings oscillating predominantly in a single mode envisioned a two-stage analysis, where the first stage involved the non-linear static analysis of the MDOF system using alternative monotonically increasing lateral load patterns and the second stage involved the non-linear time-history analysis of the equivalent SDOF system. Today, the N2 method constitutes the backbone of Eurocode 8 and the Italian building Code (NTC2018) as far as it regards the seismic design and assessment of buildings. In the code-based approach, the equivalent SDOF system is defined as an elastic-perfectly-plastic model and the structural analysis is performed through the inelastic design spectrum. On the other hand, non-linear dynamic time-history analysis of the MDOF system subjected to un-scaled ground motion records, better known as the Cloud Analysis, is noteworthy due to its simplicity, relatively small number of records employed, and its preservation of the original frequency content. A modified version of the Cloud Analysis can effectively consider the cases of structural collapse and/or numerical non-convergence. This modified version of the Cloud Analysis proves ideal for implementation in the context of the N2 method and the code-based provisions since it can be applied as a dynamic analysis procedure directly to the code-based equivalent elastic-perfectly-plastic SDOF model. This method can be applied for seismic design and assessment both for the serviceability and the ultimate limit states. The proposed non-linear dynamic analysis procedure is applied to a frame belonging to a pre-seismic code school building in Avellino (Campania), located in southern Italy. The frame is modelled by considering the interaction between the shear, axial force and flexure and the rigid-end rotation due to bar slip.

1 INTRODUCTION

The Italian Building Code (NTC 2018) outlines a detailed procedure for non-linear static analysis of buildings (NTC 2018 Commentary, C7.3.4.2). In this procedure, the capacity curve or the static pushover curve are obtained by plotting the base-shear versus a designated control displacement (e.g., rood drift, roof displacement) for a structure that is subjected to prescribed monotonically increasing static load patterns. The prescribed load patterns are used in order to map the capacity curve for the structure into an equivalent SDOF system. This is in line with the original N2 method (Fajfar and Fischinger 1988) and its later versions (e.g., Fajfar 2000). The code provides a detailed procedure for finding an

elastic-perfectly-plastic (EPP) equivalent single-degree-of-freedom (SDOF) system. The target displacement (a.k.a., the performance point) for the equivalent SDOF system is found by intersecting the inelastic design spectrum for a prescribed limit state and the equivalent EPP capacity curve.

The original N2 method implies that the equivalent SDOF system can also be analysed using the non-linear dynamic time-history analysis. However, the code provides the option for non-linear time-history analysis only for the multi-degree-of-freedom (MDOF) structure (NTC2018, §7.3.5). The present work investigates the use of a non-linear dynamic time-history analysis known as the Cloud Analysis (e.g., Cornell et al. 2002, Jalayer et al. 2015, 2017) for the equivalent code-based SDOF

system. In particular, a modified version of the Cloud Analysis (Jalayer et al. 2017), which addresses explicitly the cases of global instability or numerical non-convergence under the auspices of the so-called "collapse" cases, is employed. This version is going to be particularly useful for analysis of systems with degrading backbone as it permits the analysis of the equivalent EPP system but filters out, in the post-processing, the cases that go beyond a designated collapse threshold.

The code asks for detailed safety-checking of the structure at the target displacement (mapped back to the MDOF level). It is shown that by employing the Modified Cloud Analysis for the equivalent SDOF system, even the safety-checking can be performed at the level of the equivalent SDOF system. This is made possible by using a system-level damage measure expressed in a critical demand to capacity format. The critical demand to capacity format permits the mapping of damage at the component level to the system level. In other words, it makes it possible to adopt a compatible definition for limit states' thresholds at the component, system and the equivalent SDOF levels.

As a case-study, an intermediate moment-resisting frame of an existing RC school structure located in Avellino (Campania Region) is employed. It is worth mentioning that the school structure in question has been subjected to major repairs. We have considered the structure in its pre-repair condition. This case-study has been the subject of several other research efforts by the authors (e.g., Jalayer et al 2010, 2011, and 2015). Herein, a new non-linear model of the frame is used in which the interaction between flexure, shear and the axial forces and the rigid end rotation due to bar slip are explicitly modelled.

2 METHODOLOGY

2.1 The equivalent SDOF and the limit states

Consider the equivalent SDOF system that is derived based on the static pushover analysis on the MDOF structure and a given load pattern in Fig. 1 (see Commentary of NTC 2018, C7.3.4.2., and Fajfar 2000). The limit states are defined at the MDOF level based on NTC 2018 commentary C8.7.1.3 as follows: limit state of immediate occupancy (**SLO**, green circle); limit state of damage (**SLD**, yellow circle); limit state

of life safety (**SLV**, magenta square) and the limit state of near collapse (**SLC**, red triangle).
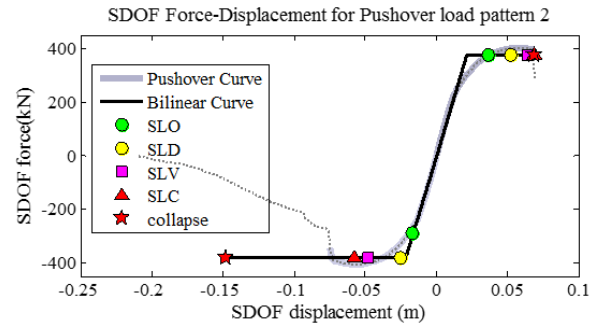
Figure 1: Equivalent SDOF system (the thick grey line); the equivalent EPP system (solid black line) and the NTC2018 serviceability and ultimate limit states

The point marked as collapse (red star) is calculated as the point on the original pushover curve where more than 50% of the columns in a given floor lose their load-bearing capacity (Galanis and Moehle 2015, Jalayer et al. 2017).

2.2 The system-level damage measure (DCR)

In this study the onset of a given limit state is quantified by employing a system-level damage measure defined for a prescribed limit state as the critical demand to capacity ratio (DCR_{LS}) for the component that takes the structure closest to the onset of the limit state (Jalayer et al. 2017). In other words, DCR_{LS} is expressed in a fully deformation-based manner as the maximum of DCR_{LS} values for all the structural elements expressed as the ratio of chord rotation demand to chord rotation capacity for that limit state. The component chord rotation capacities are derived directly from section analysis and aggregation of the flexural-axial, shear, and fixed end rotation contributions on the element level. Fig. 2 shows the onset of **SLO**, **SLD**, **SLV**, **SLC** and the "collapse" point on the force-displacement curve for flexure-driven (Fig. 2, top) and shear-flexure-critical (Fig. 2, bottom) column elements. The concept of demand to capacity ratio can also be extended to the equivalent EPP system at the SDOF level. The DCR^*_{LS} can be defined in a straight-forward manner as the ratio of the displacement demand for the equivalent SDOF system and the displacement at the onset of limit state LS that is mapped to the SDOF level.
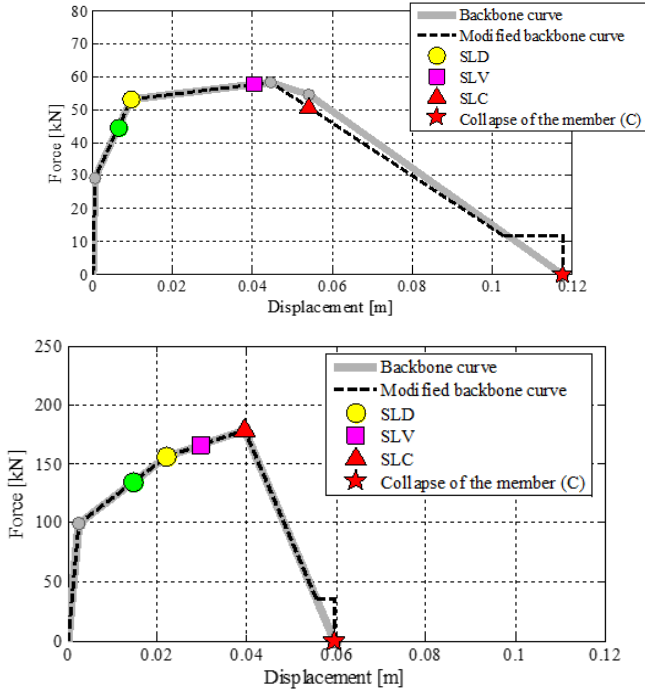
Figure 2: Examples of force-displacement curve calculated based on aggregated section analysis: (**top**) flexure-driven behaviour); (**bottom**) shear-flexure-critical behaviour. The component capacities for **SLO** (yellow circle), **SLD** (green circle), **SLV** (magenta square), **SLC** (red square) and loss of load-bearing capacity (red star) are marked on the figure.

2.3 N2 with Cloud Analysis

A modified version of the Cloud Analysis introduced in Jalayer et al. (2017) is employed herein for the equivalent single-degree-of-freedom EPP system (hereafter referred to as *Modified Cloud Analysis*, MCA). The MCA formally considers the structural response to collapse-inducing records, signaled herein by occurrence of DCR^{*}_{LS} values larger than the DCR value at the onset of "Collapse" for the equivalent EPP system (the red star in Fig. 1). Let the Cloud data, consisted of the pairs of ($DCR^{*}_{LS,i}$, Sa^{*}_i), i=1:N for the suite of selected N records, be partitioned into two parts: (a) NoC data which corresponds to that portion of the suite of records for which the structure does not experience "Collapse", (b) C data corresponding to the "Collapse"-inducing records. It is interesting to note that the pth percentile of the performance variable given Sa can be expressed as:

$$DCR^p(Sa = x) =$$
$$DCR_{NoC}(x) \cdot \exp\left(\beta_{DCR|Sa,NoC} \cdot \Phi^{-1}\left[pN/N_{NoC}\right]\right) \quad (1)$$

where DCR^p is the pth percentile of the damage measure as a function of the seismic intensity Sa;

$DCR_{NoC}(x)=a \cdot x^b$ is the median demand to capacity ratio for the non-collapse portion of the data as a function of the seismic intensity; Φ^{-1} is the inverse function of standardized Normal cumulative density function; $\beta_{DCR|Sa,NoC}$ is the standard error of logarithmic regression defined as:

$$\beta_{DCR|Sa,NoC} = \sqrt{\frac{\sum_{i=1}^{N_{NoC}} \ln\left(\frac{DCR_{LS,i}}{a \cdot Sa_i^b}\right)^2}{N_{NoC} - 2}} \quad (2)$$

The constants ln$a$ and b are the linear least square regression coefficients of DCR_{NoC} versus Sa=x regression in the natural logarithmic scale, and N_{NoC} is the number of non-collapse inducing records. The probability of no collapse given intensity can be estimated (roughly) as N_{NoC}/N, where N is the total number of records. Note that the above formulas can be applied at both MDOF and SDOF levels. The Sa at the MDOF level is the first-mode spectral acceleration and at the SDOF level is the elastic spectral acceleration at the equivalent period T^*. Furthermore, DCR^{*}_{LS} at the SDOF level is equal to the ratio of the displacement demand for the equivalent SDOF system normalized by the displacement at the onset of LS (mapped from the pushover curve into the SDOF level). Meanwhile, DCR_{LS} at the MDOF level is the critical demand to capacity ratio for the structure for limit state LS as defined in the previous sections. It is to note that the median DCR_{LS} curve corresponds to p=0.50 and the 16th percentile corresponds to p=0.16 (the N2 with Cloud Analysis procedure is visualized later in the numerical example section).

2.4 Safety-checking

A first-order (non-conservative, see e.g., Jalayer et al. 2007) effort to do safety-checking at the SDOF level would be to calculate the median DCR^{*}_{LS} value (from the curve in Eq. 1 with p=0.50) corresponding to the elastic spectral acceleration at T^* value from the design spectrum of the prescribed LS. If such value is greater than unity, the structure is not going to verify the prescribed limit state. Obviously, similar considerations can be made at the MDOF level. However, the scope of this paper is to introduce a very efficient non-linear dynamic analysis method suitable for the code-based equivalent EPP system. It is case of mentioning that the code

adopts the method of partial safety coefficients (a.k.a., the semi-probabilistic method) for material properties and resistances. Herein, we aim at eventual implementation of a fully probabilistic method (something similar to approach adopted in Cornell et al. 2002) for safety-checking. Therefore, we have not applied the partial safety factors for the materials nor the confidence factor. Nevertheless, as it will be stated later, the load factors have been assigned according to the code provisions.

3 NUMERICAL EXAMPLE

3.1 The Structural Model

One of the frames in an existing pre-seismic code school building located in Avellino (Campania), Italy is considered for the application.
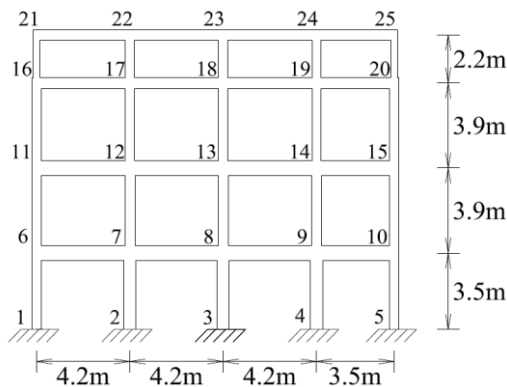
Figure 3: The RC moment-resisting frame considered in the application

The case-study structure consists of three stories with a semi-embedded story. the average shear wave velocity of the upper 30m, V_{S30}, is calculated around 470 m/sec; hence, the structure lies on soil type B (according to national Italian code NTC 2018 site classification, $360m/sec < V_{S30} < 800m/sec$). The building is constructed in the 1960s and is designed for gravity loads only. The structure is composed of bi-dimensional parallel frames, without transversal beams. The main central frame in the structure is used herein as structural model (see Fig. 3). The columns have rectangular sections with the following dimensions: first storey, $40 \times 55cm^2$ mid-columns and $40 \times 40cm^2$ side-columns; second storey, $40 \times 45cm^2$ mid-columns and $30 \times 40cm^2$ side-columns; third storey,

$40 \times 40cm^2$ mid-columns and $30 \times 40cm^2$ side-columns; forth storey, $30 \times 40cm^2$ mid-columns and $30 \times 30cm^2$ side-columns. The beams, also with rectangular section, have the following dimensions: $40 \times 70cm^2$ at first and second storey, and $30 \times 50cm^2$ for the ultimate two floors. The finite element model of the frame is constructed, using OpenSees (http://opensees.berkeley.edu, version 2.5.0), assuming a distributed placidity model by employing a beam-with-hinges element (Scott and Fenves 2006) from the library of OpenSees. This element is used to model the member-end plasticity with the capability of spreading the plasticity beyond the plastic hinge regions. As the uniaxial material from OpenSees library, Pinching4 material is used. The points on the backbone curve (shown in Fig. 2) are defined as follows. The moment-curvature analysis of beam-column elements subjected to flexure and axial force is performed and the lateral force-deformation response of the element is obtained by considering the flexural-compression response of the element (section analysis for normal stresses). This spring is acting in series with a shear spring and a spring representing the fixed-end rotations (bar-slip). The total lateral force-deformation response of the element considers the interaction between the shear, bar-slip and the axial-flexural response. The material properties for rebars and concrete are characterized based on original design documents and the available in-situ test results (i.e., the tension test, the core tests, the ultrasonic test, and pacometric and geo-radar tests, see Petruzzelli et al. 2010, and Ebrahimian and Jalayer 2019 for details). It is to note that the confidence factor (our knowledge of the building is compatible with knowledge level 2) and the partial safety coefficients are not taken into account (i.e., they are all set to unity). It is to note that the load factors for gravity loading in the seismic load combination are assigned according to the NTC (§2.5.3, Table 2.5.1) for the class of use of the building (School, Class III). Specifically, the dead load (G) factor is equal to unity and the live load (Q) factor is equal to 0.6.

3.2 The set of ground motion records

For the purpose of illustration of results, we selected a large ground motion set of 160 records from NGA West2 Database (Ancheta et al. 2014), ITACA (Italian Accelerometric Archive), and recent Iranian recordings (International Institute of Earthquake Engineering, IIEES, *personal*

communication). It is to mention that meaningful results can be obtained even with a very smaller set of records (in the order of 10 to 30). In fact, the NTC2018 (§7.3.5) recommends the selection of only 7 ground-motion records for a bi-dimensional structural model.
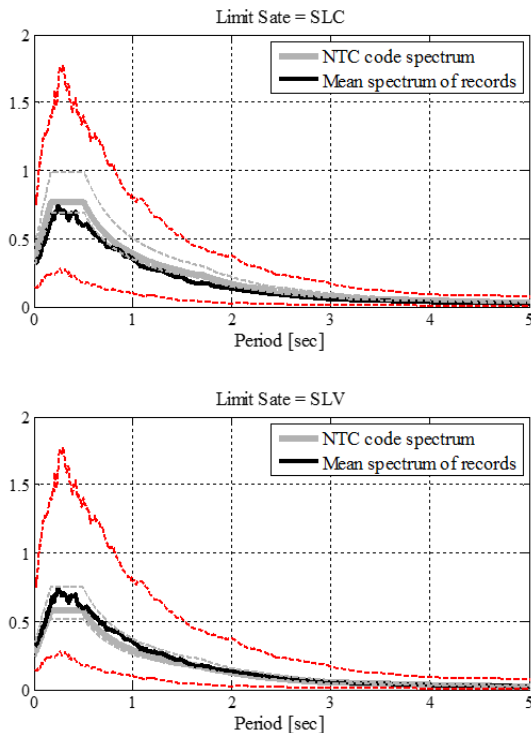
Figure 4: The mean (solid black line) and 16th and 84th percentile spectra (red dashed lines) for the suite of 160 records and comparison with the NTC2018 design spectra (the thick solid grey line) for **SLV** (**top**) and **SLC** (**bottom**). The code limit for spectrum compatibility are shown (grey dashed lines).

Clearly, since the computational effort for the analysis of a EPP single degree of freedom system is minimum, we took the liberty of choosing a large record set. The set of records are spectrum compatible for **SLV** and **SLC** (the mean spectrum falls within the limit established by the code in §3.2.3.6, see Fig. 4). The selected records have $180m/s < V_{s30} < 720m/s$ (corresponds to NTC soil types B and C), moment magnitude greater than 5 (no limits on the source-to-site distance is considered). The records correspond to crustal focal mechanisms (reverse, strike-slip and normal faulting styles) and no more than 6 recordings from the same earthquake events have been chosen. We have been particularly careful in maximizing the dispersion around the mean spectrum. Large dispersion in spectral acceleration values (the independent regression variable in Cloud Analysis) favours a more accurate estimation of the slope of regression.

Moreover, the code seems to provide specifications only about the mean spectrum with respect to the design spectrum and no specific provisions are provided for record-to-record variability. It is to note that the code spectra are derived for Class III (schools).

3.3 Non-linear static analysis according to NTC2018

The static pushover has been done following the provisions in the code (C7.4.3.2, NTC2018 Commentary) by adopting two different load patterns; namely, first-mode-shape proportional (*pattern 1*) and proportional to the inertial forces (*pattern 2*) in two different directions. Figure 5 shows the pushover curve (base shear versus roof displacement as the "control" displacement).
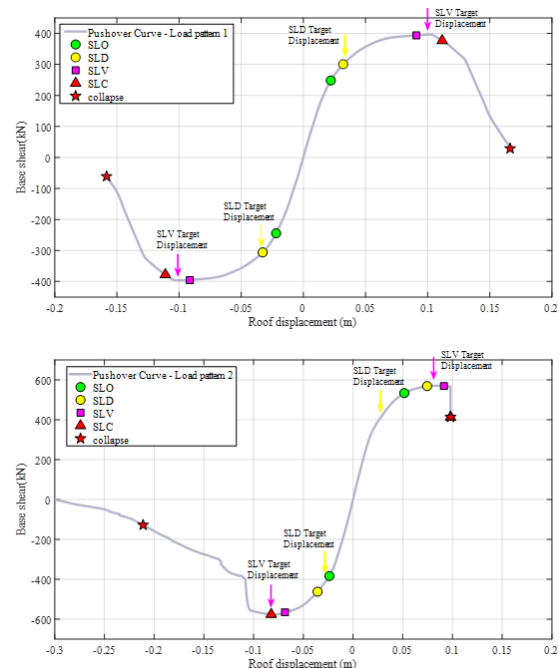
Figure 5: Base shear versus roof displacement for load pattern 1 (**top**, first-mode shape) and load pattern 2 (**bottom**, mass proportional). The target displacement for limit states of **SLD** and **SLV** are shown with arrows of the same colour as that of the corresponding limit states.

The target displacements are calculated by intersecting the inelastic spectrum and the capacity curve for the SDOF equivalent EPP system, as instructed by the code, for the two limit states of **SLD** (serviceability) and **SLV** (ultimate) for the sake of demonstration. It is interesting to note that, a compatible definition and mapping of the limit states' thresholds from the component-level to the system-level makes it possible to do the code-based safety-checking visually and at the system level. It can be

observed that the frame in question does not verify the life safety limit state. It marginally verifies the damage limit state. Nevertheless, since the confidence factor and the partial safety factors are not taken into account, the safety-checking is leaning to the non-conservative side. Therefore, the frame is not satisfying the SLD limit state.

3.4 Non-linear time-history analysis according to NTC2018

We have chosen two different subsets of 7 records (from the original pool of 160 ground motions described in Section 3.2) according to the code (NTC2018 §7.3.5 and §3.2.3.6) and have ensured spectrum compatibility for **SLD** and **SLV** limit states within a period range of $0.20T_1$ and $1.5T_1$ (see Fig. 6; note that T_1=0.84 sec is the first-mode period for the frame). Table 1 in its third row shows the average maximum roof drift for the structure subjected to the two suites of records for the two limit states of **SLD** and **SLV**. For safety checking purposes, we normalized the two values by the corresponding limit state thresholds marked on the pushover curves in Fig. 5. It can be observed that the two demand to capacity ratios for the limit states of damage and life safety are larger than one. Therefore, the frame does not satisfy the two limit states. It is also interesting to note that the results are perfectly compatible with those of the static non-linear analysis.

3.5 N2 with Cloud

Fig. 7 shows the results of MCA on the set of 160 ground motions for the limit states of life safety (**SLV**) and damage (**SLD**). The records are applied to the equivalent EPP system without being scaled. It is to note that the same set of records are applied for **SLV** and **SLD** (the spectrum compatibility is ensured only for the ultimate limit states). It is also noteworthy that the structural analyses are done only once; the different between the two limit states is only reflected in the normalization for calculating the DCR^*_{LS} thresholds and the post-processing of the MCA results for getting the percentiles curves according to Eq. 1. Both plots show the median DCR^*_{LS} values as a function of the elastic spectral acceleration at the period of the equivalent SDOF system T^*, $Sa(T^*)$. Also the 16th percentile curves are shown on both graphs.
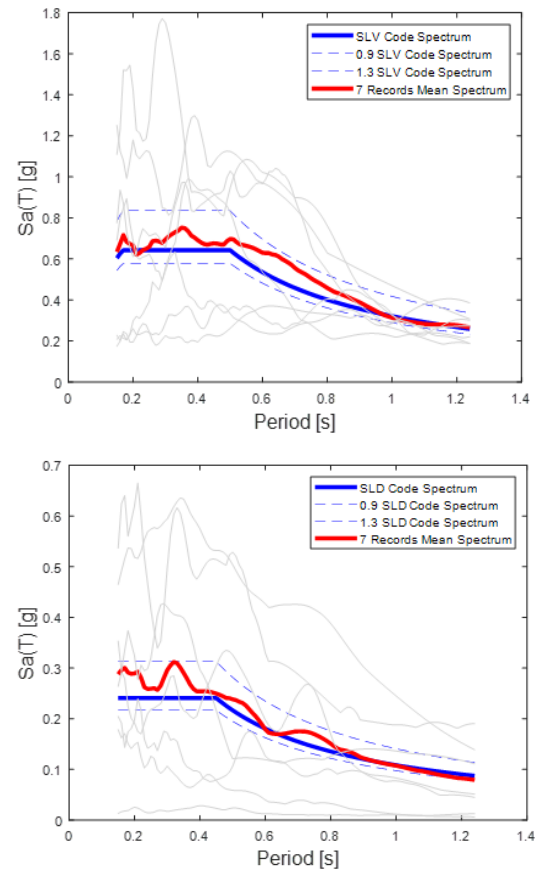
Figure 6: NTC spectrum-compatible records for **SLV** (**top**) and **SLD** (**bottom**).

Eventually, the distance between the 50th and 16th percentile curves can be used for calculating equivalent standard deviation of the $Sa(T^*)$ at the onset of the limit state (DCR^*_{LS}=1). This latter quantity is a key parameter for fully probabilistic safety-checking (out of the scope of this conference paper). It important to stress that the analyses are done on the EPP defined on the equivalent SDOF. The effect of the degrading backbone of the frame (which eventually leads to the loss of load-bearing capacity, the red stars in Fig. 1, Fig. 2 and Fig. 5) is considered in the post-processing phase (MCA, Eq. 1).
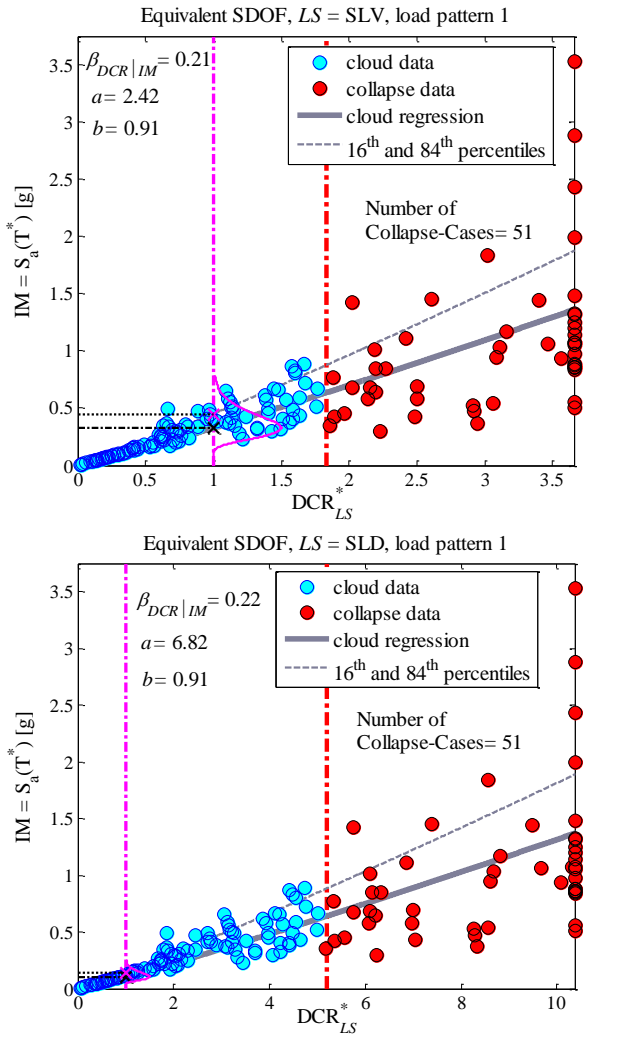
Figure 7: The results of modified Cloud Analysis for **SLD** and **SLV** limit states. The limit state threshold DCR^*_{LS}=1 is shown as the pink dashed-sot line. The DCR^*_{LS} threshold for "collapse" is shown as the red dashed-dot line. The logarithmic regression coefficients a, b, $\beta_{DCR|Sa}$ are shown on this figure. The median (Eq. 1, p=0.50 curve) is shown as a thick grey line and the 16th percentile (Eq. 1, p=0.16 curve) is shown a as a dashed grey line.

3.6 N2 with Cloud: Safety-checking

Fig. 8 and Fig. 9 illustrate the safety-checking procedure for both limit states of **SLV** and **SLD**. It can be seen that for each limit state, the elastic spectral acceleration is calculated at T^*=0.89 sec (the period of the equivalent EPP system). This spectral acceleration can be viewed as a proxy for the seismic demand intensity. It is to note that the code spectrum is calculated for a reference lifetime of V_R=75 years (50 years times C_U=1.5, NTC2018 Tables 2.4.I and 2.4.II). The acceptable probability of at least one limit state exceedance in the reference lifetime for **SLD** and **SLV** is equal to P_o=63% and P_o=10%, respectively. These probabilities correspond to return periods equal to 75 years and 711 years for **SLD** and

SLV, respectively. It can be seen that for both limit states, the median DCR^*_{LS} value is greater than unity and the structure does not verify for neither **SLD** nor **SLV**. As mentioned before, these verification are on the non-conservative side as the effect of record-to-record variability and the structural modelling uncertainties are not considered herein. Nevertheless, considering only the median DCR provides a first-order approximation to the expected value for the demand to capacity ratio for the structure.
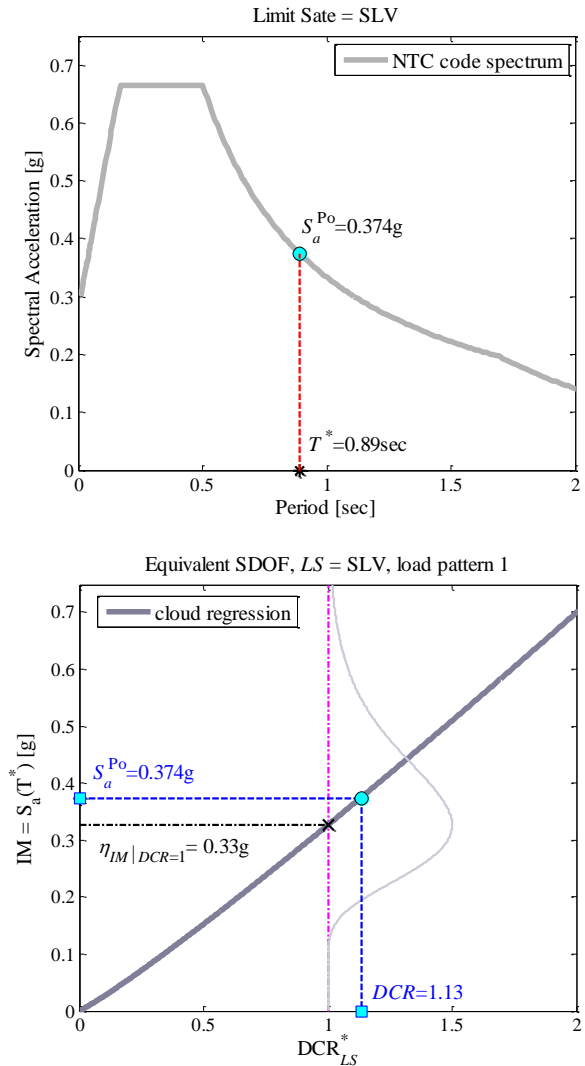
Figure 8: (**top**) the elastic spectral acceleration spectrum for NTC2018, **SLV**. The spectral acceleration at T^* is shown as blue circle (Sa^{Po}); (**bottom**) the median DCR is calculated at Sa^{Po}.
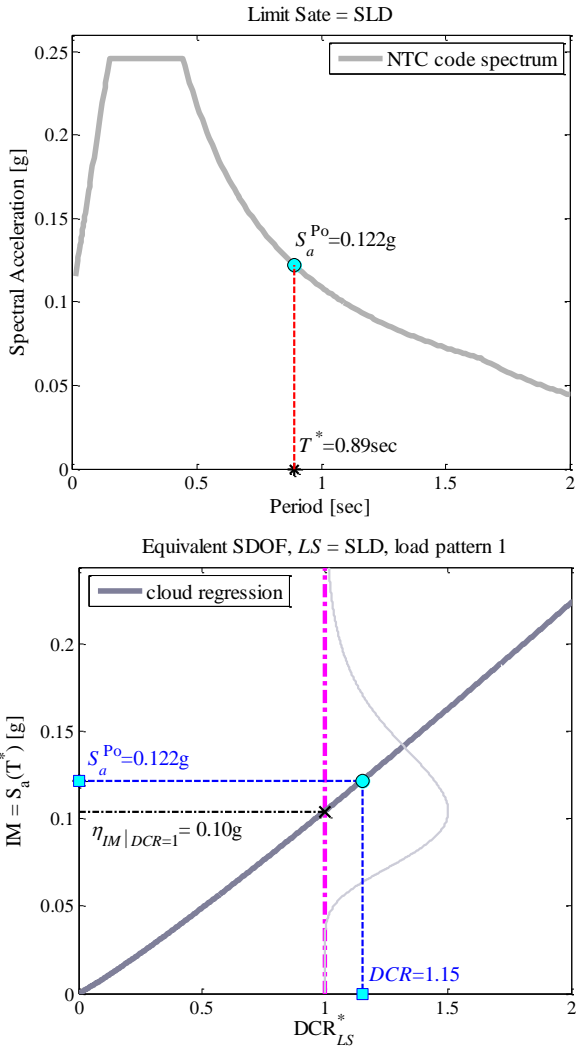
Figure 9: (**above**) the elastic spectral acceleration spectrum for NTC2018, **SLD**. The spectral acceleration at T^* is shown as blue circle (Sa^{Po}); (**below**) the median DCR is calculated at Sa^{Po}.

3.7   Modified Cloud Analysis for the MDOF

Representing a "*golden-truth*" herein, the MCA has also been performed for set of 160 ground motion records applied to the original MDOF frame. Fig. 10 illustrates the results. It should be noted that a slightly modified version of the MCA analysis is used here (see Jalayer et al. 2017) for more detail. More specifically, the "collapse" points are characterized directly by post-processing the structural analysis results as cases in which more than 50% of the columns in a given floor have lost their load bearing capacity.

The DCR values, as mentioned before, are the demand to capacity ratios (calculated in terms of the chord rotation at the element level) for the element that brings the structure closest to the onset of the prescribed limit state. The percentile curves for DCR as a function of Sa are calculated according to a more advanced version of Eq. 1

that uses the logistic regression for calculating the probability of *NoC* cases. Comparing the results (the *NoC* part of the two Cloud Analyses are plotted as blue circles) in Fig. 10 with those of Fig. 7, a higher degree of higher variability can be observed in the MDOF Cloud data, especially for smaller intensity values. This somehow underlines the effect of higher modes on the dynamic response of the moment resisting frame.
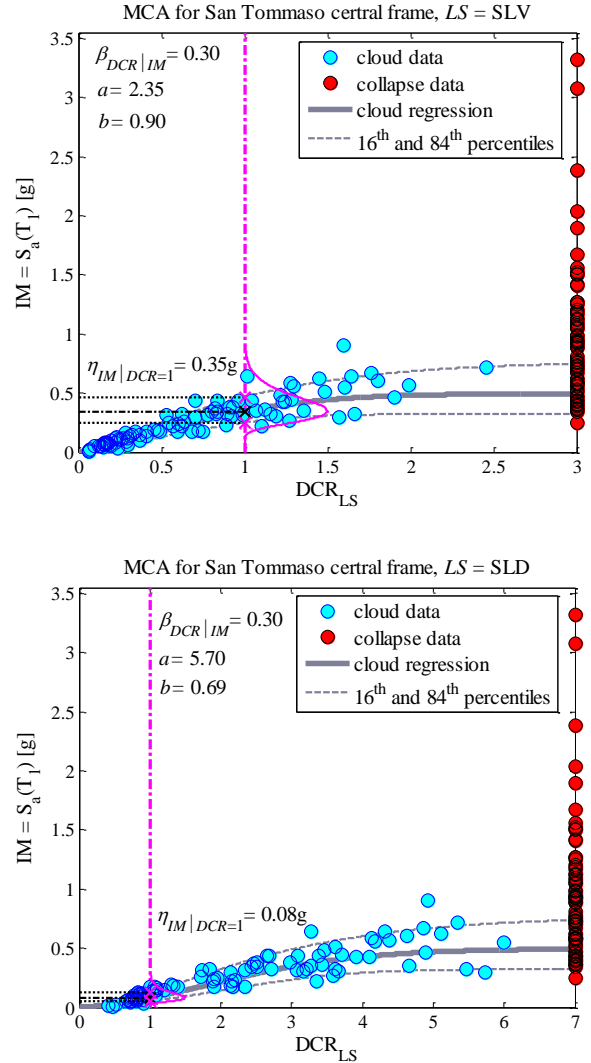
Figure 10: The results of MCA for **SLV (top)** and **SLD (bottom)** limit states for the MDOF moment resisting frame considering the flexural-shear-axial interactions and the bar-slip. The limit state threshold DCR_{LS}=1 is shown as a red dashed-dot line. The "collapse" points are shown as red circles. The logarithmic regression coefficients a, b, $\beta_{DCR|Sa}$ are shown on the figure. The median (Eq. 1, p=0.50 curve) is shown as a thick grey line and the 16th and 84th percentiles (Eq. 1, p=0.16 and p=0.84 curves) are shown as dashed grey lines.

3.8   Synthesis of results

Table 1 provides a synthesis of various safety-checking methods discussed herein. In the first place, the table reports the (worst case) target roof ratios for the limit states of **SLV** and **SLD** for

pushover load patterns 1 and 2, obtained directly from the pushover curves (see Fig. 5). These target values are obtained by mapping back the target displacement calculated according to the code specification (the inelastic spectrum versus EPP capacity curve) to the MDOF level. The third row shows the results (i.e., mean roof drift) of non-linear time-history analysis for the two sets of **SLV** and **SLD** spectrum compatible records (as shown in Figure 6). The table also reports the DCR_{LS} calculated as the mean roof displacements normalized to the **SLV** and **SLD** limit states' thresholds from the pushover curve (Pattern 1). The table illustrates in its forth row the DCR_{LS} values calculated from the proposed N2 with Cloud procedure based on the set of 160 ground motion records for both limit states. Finally, the last row reports the "golden truth" DCR_{LS} values calculated directly by performing MCA on the moment-resisting frame in question. It can be seen that, although providing different *DCR* values (which in turn are defined differently), all the methods lead to the same conclusions regarding safety-checking for the both limits states.

	SLD		SLV	
	Target	DCR_{SLD}	Target	DCR_{SLV}
Pushover (Pattern 1)	0.034 m	1.05	0.100 m	1.10
Pushover (Pattern 2)	0.028 m	0.73	0.082 m	1.17
7 GM (mean)	0.030 m	1.13	0.093 m	1.07
N2-Cloud 160 GM		1.15		1.13
MCA, MDOF 160GM		1.33		1.06

Table 1: Safety-checking according to the alternative methods discussed herein.

CONCLUSIONS

A non-linear dynamic analysis method suitable for the Italian code-defined equivalent elastic-perfectly-plastic system dubbed as "N2 with Cloud" is discussed. This method is suitable for implementation in a fully probabilistic performance-based framework for assessment and safety-checking of existing structures. There are several advantages associated to the proposed method:

- o The structural model is a simple EPP system. Therefore the running time and the analysis complications are going to be minimal.
- o Although the model is a EPP; the results are post-processed in order to mark the cases which go beyond the load-bearing capacity of the original structure. Arguably, this can be considered as a

proxy for consideration of the degrading backbone behaviour for an existing structure.

- o The obtained results are readily usable in the context of performance-based assessment framework. That is, they can be used for fragility and risk calculations.
- o In particular, these results can be directly implemented in the Demand and Capacity Factors Design (DCFD, Cornell et al. 2002, Jalayer and Cornell 2003) safety-checking format.
- o This paper shows a first-order approximation to safety-checking with DCFD based on the results of N2 with Cloud.

However, there are some limitations to keep in mind:

- o The effect of hysteresis behaviour with pinching is not considered.
- o The method inherits some of the limitations of the non-linear static procedure in the code (NTC 2018 Commentary, C7.3.4); that is, it can be used for relatively regular and first-mode dominant structures.
- o Using this method in a fully probabilistic context for existing buildings (considering structural modelling uncertainties) needs some extra attention (which is not discussed in this paper).

REFERENCES

Ancheta, T. D., Darragh, R. B., Stewart, J. P., Seyhan, E., Silva, W. J., Chiou, B. S. J., ... & Kishida, T. (2014). NGA-West2 database. Earthquake Spectra, 30(3), 989-1005.

Cornell, C. A., Jalayer, F., Hamburger, R. O., & Foutch, D. A. (2002). Probabilistic basis for 2000 SAC federal emergency management agency steel moment frame guidelines. Journal of structural engineering, 128(4), 526-533.

Ebrahimian H., Jalayer F., 2019. In-situ tests and inspections for reliability assessment of RC buildings: How accurate? *XVIII Convegno l'ingegneria sismica in Italia (ANIDIS)*, Ascoli Piceno, 15-19 September.

Fajfar, P., and Fischinger, M. (1988, August). N2-A method for non-linear seismic analysis of regular buildings. In

Proceedings of the ninth world conference in earthquake engineering (Vol. 5, pp. 111-116).

Fajfar, P. (2000). A nonlinear analysis method for performance-based seismic design. Earthquake spectra, 16(3), 573-592.

Galanis, P. H., & Moehle, J. P. (2015). Development of collapse indicators for risk assessment of older-type reinforced concrete buildings. Earthquake Spectra, 31(4), 1991-2006.

Jalayer, F., Franchin, P., & Pinto, P. E. (2007). A scalar damage measure for seismic reliability analysis of RC frames. Earthquake Engineering & Structural Dynamics, 36(13), 2059-2079.

Jalayer, F., Iervolino, I., & Manfredi, G. (2010). Structural modeling uncertainties and their influence on seismic assessment of existing RC structures. Structural safety, 32(3), 220-228.

Jalayer, F., Elefante, L., Iervolino, I., & Manfredi, G. (2011). Knowledge-based performance assessment of existing RC buildings. Journal of Earthquake Engineering, 15(3), 362-389.

Jalayer, F., De Risi, R., & Manfredi, G. (2015). Bayesian Cloud Analysis: efficient structural fragility assessment using linear regression. Bulletin of Earthquake Engineering, 13(4), 1183-1203.

Jalayer, F., Ebrahimian, H., Miano, A., Manfredi, G., & Sezen, H. (2017). Analytical fragility assessment using unscaled ground motion records. Earthquake Engineering & Structural Dynamics, 46(15), 2639-2663.

Italian Accelerometric Archive (ITACA), http://itaca.mi.ingv.it/ItacaNet_30/#/home (last accessed 19.07.2019)

NTC 2018: Supplemento ordinario alla Gazzetta Ufficiale, n. 42 del 20 Febbraio 2018. Ministero delle Infrastrutture e dei Trasporti, DM 17 Gennaio 2018 "*Aggiornamento dell Norme tecniche per le costruzioni*".

NTC 2018 Commentary: Supplemento ordinario alla Gazzetta Ufficiale, n. 35 del 11 Febbraio 2019. Ministero delle Infrastrutture e dei Trasporti, Circolare 21 Gennaio 2019 "Istruzioni per applicare dell' *«Aggiornamento delle Norme tecniche per le costruzioni» di cui al decreto ministeriale 17 Gennaio 2018*".

Petruzzelli, F., Jalayer, F., Iervolino, I., & Manfredi, G. (2010). Accounting for the effect of in-situ tests and inspections on the performance assessment of existing buildings. In Proceedings of 14th European Conference on Earthquake Engineering, Ohrid, Macedonia.

Scott, M. H., & Fenves, G. L. (2006). Plastic hinge integration methods for force-based beam–column elements. Journal of Structural Engineering, 132(2), 244-252.